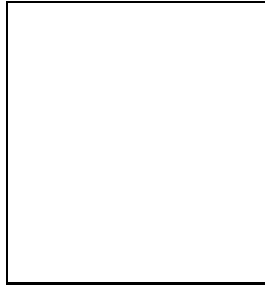


Strangeness Production at the HERA-B Experiment.

M. Zavertyaev for the HERA-B collaboration
*Max-Planck Institut für Kernphysik, Saupfercheckweg 1,
 69117 Heidelberg, Germany.*



HERA-B is a fixed target experiment at the 920 GeV HERA proton beam at DESY which uses a variety of nuclear targets. During the last data taking period from Nov. 2002 to Feb. 2003, 200 million minimum bias events were recorded. A large sample of $V^0(K_s^0, \Lambda, \bar{\Lambda})$, approximately 20000 cascade hyperons Ξ^\mp and 1200 Ω^\mp over low background were reconstructed using these data. About 1 million $K^*(892) \rightarrow K\pi$ and 60,000 $\phi(1020) \rightarrow K^+K^-$ decays in central production ($-0.15 < x_F < 0.1$, $0.5 < p_t^2 < 12.1$ (GeV/c) 2) were analyzed. Preliminary results for differential p_t^2 spectra, A -dependence and anti-particle to particle ratios are presented.

1 Introduction

For more than 50 years, the production of strange particles was studied in a variety of beams for a wide energy range from few MeV up to $\sqrt{s_{NN}} \sim 200$ GeV (see references in ^{1,2,3}). The production of the strange quark and its subsequent hadronization in hadron-nucleus collisions constitutes an important benchmark test for QCD-based models such as PYTHIA, FRITIOF and QCD-inspired phenomenological models ^{4,5} describing soft phenomena and for the applicability of perturbative QCD to hard processes. But even now the comparison of experimental results with existing models like PYTHIA and Quark Gluon String Model (QGSM) shows qualitative agreement only ².

A huge sample of minimum bias data collected in proton-nucleus collisions at the HERA-B experiment permits to contribute to strange particle production studies. HERA-B is a fixed target experiment at the 920 GeV proton storage ring HERA at DESY. It is a forward magnetic spectrometer with a large acceptance. It consists of a high-resolution silicon vertex detector (VDS), drift chambers (DC), a Cherenkov ring image detector (RICH), an electromagnetic calorimeter (ECAL) and a muon detector ¹. In this analysis, the information provided by the VDS, DC and RICH detectors was used. The data were taken with carbon, titanium and

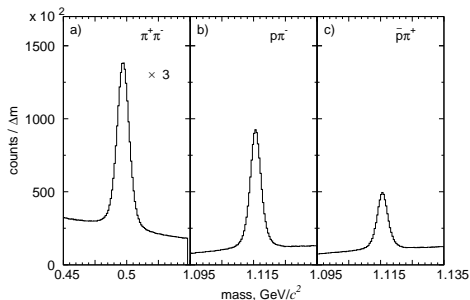


Figure 1: The invariant mass distributions for $\pi^+\pi^-$, $p\pi^-$ and $\bar{p}\pi^+$. $\Delta m = 1.0/0.4\text{MeV}/c^2$ in a)/b),c).

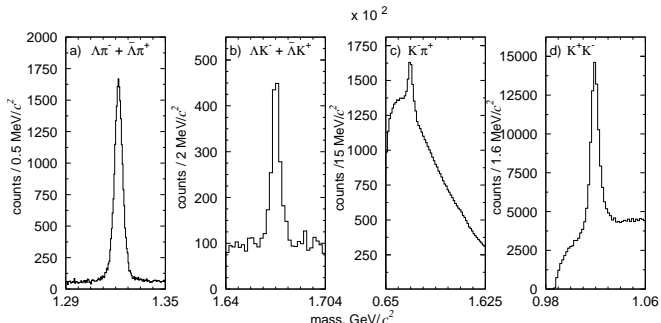


Figure 2: The invariant mass distributions for cascade hyperons (Ξ , Ω) and resonances $K^*(892)$, $\phi(1020)$.

tungsten target wires. The present study uses a sample of about 170 million events which was taken at mid-rapidity ($x_F \sim 0$).

2 Event selection

Two different classes of events were selected for the analysis. The first class is a data sample with long living particles like V^0 and the cascade hyperons Ξ^\mp and Ω^\mp . The second class includes the short living resonances $K^*(892)$ and $\phi(1020)$ selected by using particle identification by the RICH.

Only events with exactly one reconstructed primary vertex (of at least two tracks) were accepted for the analysis. In each event with at least four tracks, a full combinatorial search for V^0 candidates was performed. All pairs of oppositely charged tracks with a minimum distance smaller than 0.07 cm are considered. Clear signals of the decays of K_s^0 , Λ and $\bar{\Lambda}$ are seen above a high background. The additional cut of $p_t \cdot c\tau > 0.05\text{GeV}/c \cdot \text{cm}$ removes about 90 % of the background while the signal losses are below 5 %. No further cut on particle identification is applied. The invariant mass distributions of the $\pi^+\pi^-$, $p\pi^-$ and $\bar{p}\pi^+$ combinations are shown in Fig. 1.

The $\Lambda(\bar{\Lambda})$ candidates are accepted for further analysis if the invariant mass belongs to the region of $\pm 3\sigma$ around the peak position ($1.11\text{GeV}/c^2 < m < 1.121\text{GeV}/c^2$). The contamination from K_s^0 decays is suppressed by a cut of $\pm 3\sigma$ around the K_s^0 mass in the invariant mass spectrum ($0.482\text{GeV}/c^2 < m_{\pi^-\pi^+} < 0.512\text{GeV}/c^2$).

The invariant mass of the $\Lambda(\bar{\Lambda})$ candidates combined with one additional negative (positive) track is shown in Fig. 2a,b when this track is considered as a pion or a kaon. Clear signals of cascade hyperons are obtained by requesting that none of the decay products but only the Ξ^\mp or Ω^\mp itself must point to the primary vertex.

Signals of one million of $K^*(892)$ decays⁶ and about $5 \cdot 10^4$ $\phi(1020)$ decays⁷ were observed (Fig. 2c,d) in the invariant mass distribution of oppositely charged tracks emerging from the primary vertex with the cut on the kaon identification likelihood given by the RICH⁸. The cut on likelihood values were set at 0.3 for both kaons coming from the $\phi(1020)$ decay and 0.95 in case of $K^*(892)$. The low momentum limit for both kaons coming from the $\phi(1020)$ decay was set at $10\text{GeV}/c$.

3 Results

The analysis of the data covered the differential p_t^2 - spectra, dependency on the atomic mass of the target nucleus and anti-particle to particle ratios.

Table 1: The parameter B of the p_t^2 spectra.

	B, (GeV/c) ⁻²
K_s^0	3.6 ± 0.1
Λ	2.4 ± 0.1
$\bar{\Lambda}$	2.2 ± 0.1
Ξ^-	1.8 ± 0.2
$\bar{\Xi}^+$	1.6 ± 0.2
Ω^-	0.95 ± 0.4
$\bar{\Omega}^+$	0.93 ± 0.4

For K_s^0 the observed p_t^2 spectrum is shown in Fig. 3. For the other particles, the p_t^2 spectra look very similar. All distributions may be described by the simple Gaussian formula $d\sigma/dp_t^2 \propto \exp(-B \cdot p_t^2)$ up to $0.8-1(\text{GeV}/c)^2$ approximately. At higher p_t^2 values the spectra become flatter. The results of the fits are shown in Table 1. No significant difference was observed between the B values obtained from the different targets. The measured B values follow the general trend observed by other experiments² - the higher the mass of the particle, the wider the p_t^2 spectrum.

The p_t^2 spectra for $\phi(1020)$ and $K^*(892)$ were measured up to $12(\text{GeV}/c)^2$. A good approximation for the whole p_t^2 range of these spectra is $d\sigma/dp_t^2 \propto (1 + p_t^2/p_0^2)^{-\beta}$ in contrast to the Gaussian ansatz at low p_t^2 . The value of β for $K^*(892)$ decreases from 6 to 4.5 for C:Ti:W targets while for $\phi(1020)$ it stays constant ≈ 4.3 for all targets. The errors on the β values are from 5 to 8% .

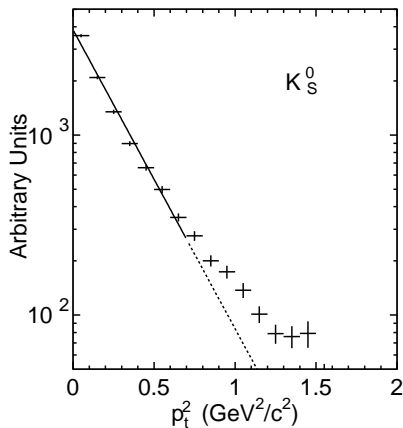


Figure 3: The differential p_t^2 production spectrum for K_s^0 on carbon nuclei.

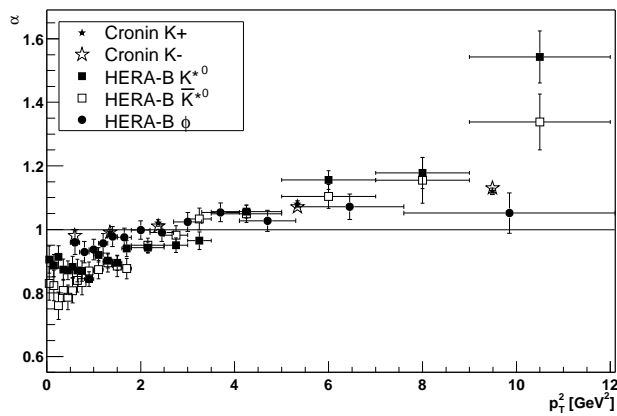


Figure 4: The ‘‘Cronin’’ effect for $\phi(1020)$ and K^* .

Fitting the p_t^2 spectra of the three materials for $\phi(1020)$ and $K^*(892)$ in each momentum intervall with the conventional formula $d\sigma_{pA}/dp_t^2 = A^\alpha \cdot d\sigma_{pp}/dp_t^2$ yields the exponent α to rise above unity at high p_t^2 (Fig. 4). This is the so-called Cronin effect which is well known for stable baryons⁹. Now effect is clearly observed also for the $\phi(1020)$ and $K^*(892)$ resonances.

The anti-particle to particle ratios at HERA-B were measured for V^0 s and cascade hyperons. The results are shown in Fig. 5. In the same plot results in Au-Au-collisions from different heavy-ion experiments are shown for comparison. The $\bar{\Lambda}/\Lambda$ ratio at HERA-B energy is about 20% smaller than at RHIC. In Fig. 6, this ratio is shown as a function of the energy. At HERA-B energies this is a rising function and at least a part of the 20% difference may be attributed to the energy dependence and not exclusively to the difference between $pA - AA$ interactions.

4 Conclusion

The minimum bias data sample taken by the HERA-B spectrometer is a source of high statistic signals of strange particles decays. On its basis studies of the p_t^2 differential production spectra were performed. The A-dependence studies show the ‘‘Cronin’’ effect for the $\phi(1020)$ and

$K^*(892)$ resonances. The comparison of the anti-particle to particle ratios in pA with the ratios in AA interactions does not show a strong difference.

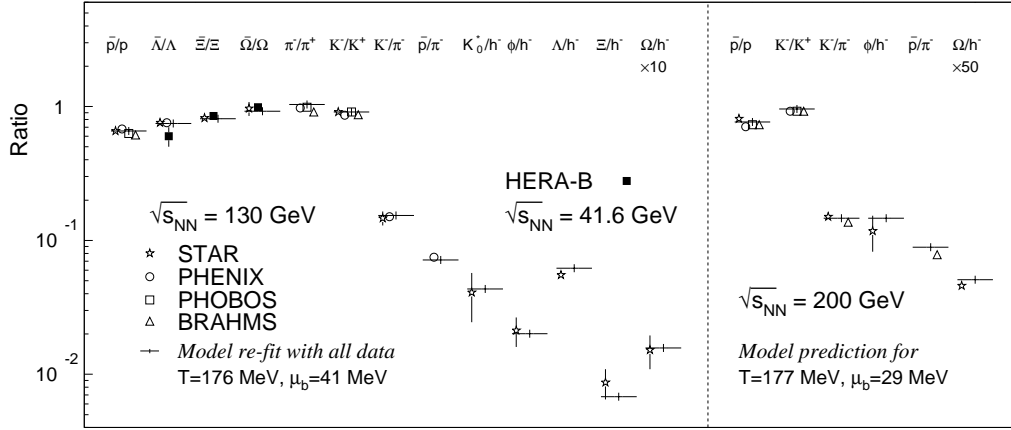


Figure 5: The anti-particle to particle ratio measured at HERA-B in comparison with the polished data ¹⁰.

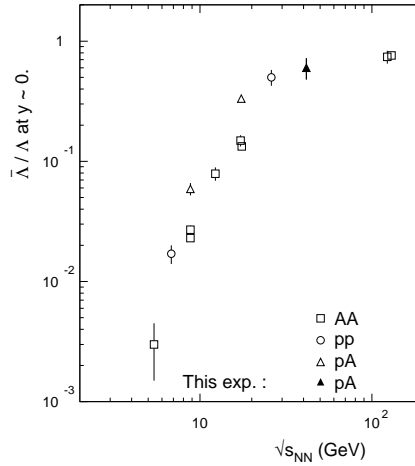


Figure 6: The anti-particle to particle ratio versus energy ¹.

References

1. I. Abt *et al.* (HERA-B collaboration), *Eur.J.Phys C* **29**, 181 (2003) and references therein.
2. M. I. Adamovich *et al.*, (WA89 collaboration), *Eur. J. Phys. C* **26**, 357 (2003) and references therein.
3. M. I. Adamovich *et al.*, (WA89 collaboration), *Z. Phys. C* **76**, 35 (1997) and references therein.
4. R.A.M.S. Nazareth, N. Prado, and T. Kodama, *Phys. Rev. D* **40**, 2861 (1989).
5. R.A.M.S. Nazareth, T. Kodama, and D.A. Portes, *Phys. Rev. D* **46**, 2896 (1992).
6. C. van Eldik, *K*0(892) production in proton-nucleus collisions*, Dissertation, University of Dortmund, March 2004.
7. M. Symalla, *Produktion von phi-Mesonen in inelastischen Proton-Kern-Wechselwirkungen*, Dissertation, University of Dortmund, March 2004.
8. I. Ariño *et al.*, *Nucl. Instr. Methods A* **516**, 445 (2004).
9. L. Kluberg *et al.*, *Phys. Rev. Lett.* **38**, 670 (1977).
10. T.S. Ullrich, *Nucl. Phys. A* **715**, 399c (2003).